Biophysical Letter

Association Rates of Membrane-Coupled Cell Adhesion Molecules

Timo Bihr,[1,2] Susanne Fenz,[3,4] Erich Sackmann,[5] Rudolf Merkel,[3] Udo Seifert,[2] Kheya Sengupta,[6] and Ana-Sunčana Smith[1,7,*]

[1]Institut für Theoretische Physik and Cluster of Excellence Engineering of Advanced Materials, Friedrich-Alexander-Universität, Erlangen, Germany; [2]II. Institut für Theoretische Physik, Universität Stuttgart, Stuttgart, Germany; [3]Institute of Complex Systems 7: Biomechanics Forschungszentrum Jülich, Jülich, Germany; [4]Department of Cell and Developmental Biology, Theodor-Boveri-Institute, Universität Würzburg, Würzburg, Germany; [5]Physics Department, Biophysics E22, Technische Universität München, München, Germany; [6]Aix-Marseille Université, CNRS, CINaM UMR 7325, Marseille, France; and [7]Institute Ruđer Bošković, Division of Physical Chemistry, Zagreb, Croatia

ABSTRACT Thus far, understanding how the confined cellular environment affects the lifetime of bonds, as well as the extraction of complexation rates, has been a major challenge in studies of cell adhesion. Based on a theoretical description of the growth curves of adhesion domains, we present a new (to our knowledge) method to measure the association rate k_{on} of ligand-receptor pairs incorporated into lipid membranes. As a proof of principle, we apply this method to several systems. We find that the k_{on} for the interaction of biotin with neutravidin is larger than that for integrin binding to RGD or sialyl Lewis^x to E-selectin. Furthermore, we find k_{on} to be enhanced by membrane fluctuations that increase the probability for encounters between the binders. The opposite effect on k_{on} could be attributed to the presence of repulsive polymers that mimic the glycocalyx, which points to two potential mechanisms for controlling the speed of protein complexation during the cell recognition process.

Received for publication 3 July 2014 and in final form 24 October 2014.

*Correspondence: smith@physik.uni-erlangen.de

Chemical reaction kinetics in the confined environment of fluctuating membranes can be very different from those in an unconstrained situation. For example, it is well established that the enthalpy for ligand-receptor binding differs significantly for events occurring in two and three dimensions (1–3). This is particularly important in the context of cell adhesion, where membrane-bound ligands react with receptors on another surface. Furthermore, although 2D dissociation rates have been extensively modeled (4–7) and measured with reasonable confidence, often in single-molecule experiments (8,9), determining the association rate seems to be more challenging (10–15). For instance, when one of the reactants is bound to a membrane (16) or the tip of a polymer (17), the thermal fluctuations of the membrane (or polymer) will determine how often the binding partners come into the interaction range, thus influencing the association rate k_{on}. Similarly, repellent polymers on one or both of the interacting surfaces will hinder the reactant encounters (14,18), thus reducing k_{on}.

We measure k_{on} for three ligand-receptor pairs in different environments: 1), the strong biotin-neutravidin pair (3D binding energy $E_b^{3D} \approx 35 k_B T$) (16), which is often used as a model but has no known physiological relevance; 2), the Arg-Gly-Asp (RGD)-$\alpha_{IIb}\beta_3$ integrin pair, which is considered strong in the context of cell adhesion ($E_b^{3D} \approx 10 k_B T$) (19); and 3), the weaker sialyl Lewis^x binding to E-selectin ($E_b^{3D} \approx 5 k_B T$) (20).

As cell models, we use giant unilamellar vesicles (GUVs) (21,22) that are functionalized with lipid-anchored ligands (biotin, RGD, or sialyl Lewis^x) of size a at an initial concentration (see Supporting Material for details). Due to the fluidity of the GUV membrane, the ligands can explore their surface with a diffusion constant $D \approx 10\ \mu m^2/s$. The corresponding receptors are fixed on a 2D planar substrate at density ρ_r. E-selectin and integrin are deposited by physisorption, whereas the neutravidin is incorporated into a solid supported bilayer, where it is nevertheless immobile at the considered densities due to crowding (23). We modulate the rate of ligand-receptor encounters by adding polymers (polyethyleneglycol (PEG)) to the GUV membrane or by increasing the membrane fluctuations after the osmotic deflation of vesicles.

In the early stages of the experiment, vesicles sediment onto the substrate and form a strongly fluctuating contact zone, which when visualized by reflection interference contrast microscopy (RICM) (24) appears as a patch of variable intensity surrounded by a few quasi-circular fringes against a gray background (Fig. 1, *top*). Experimental details can be found in the Supporting Material and Fig. S3. At some point, an adhesion domain rich in bonds nucleates

Editor: Markus Deserno.

http://dx.doi.org/10.1016/j.bpj.2014.10.033

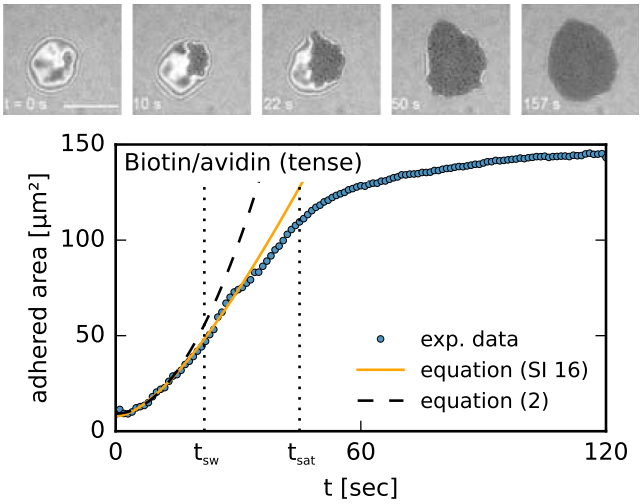

FIGURE 1 Top: RICM snapshots of a growing adhesion domain (*dark area*) mediated by biotin-avidin bonds. The scale bar is 10 μm. Bottom: experimental growth curve including fits to our theoretical results.

(as shown by a dark, homogeneous patch with strongly reduced fluctuations in RICM) and begins to grow radially outward (16,19,20). After a certain time, its area saturates due to the finite size of the vesicle (Fig. 1, *bottom*). In the case of weaker bonds, multiple seeds may form; however, such cases are not considered here because interactions between the domains could make a quantitative analysis unreliable.

Qualitatively, the same behavior was observed in a few systems with different binding pairs (20,25,26), and depending on the relative importance of viscous dissipation, membrane elasticity, and bond density and strength, several mechanisms were theoretically suggested to be responsible for the dynamics (27,28). Furthermore, two qualitatively different regimes were identified depending on the relative density of receptors and ligands. Specifically, for $\rho_l^0/\rho_r>1$, the growth of the adhesion area was quadratic in time, as expected for reaction-limited kinetics (19,29). Alternatively, for $\rho_l^0/\rho_r<1$, the area of a domain displayed a linear time dependence (19), which is consistent with the solution of the Stefan problem (29–31). By inspection of our own and previously published data (19) for which $\rho_l^0/\rho_r<1$, we notice deviations from the linear behavior at short timescales (Fig. 1). We explain this effect by reformulating the Stefan problem (see Fig. S1 and Supporting Material for details) to account for a k_{on}-dependent radiation boundary condition (Eq. S2). The full solution (Eq. S16) of this diffusion problem shows that the growth of a domain is always reaction limited in the initial stages. At later times, the growth becomes diffusion limited because the contact zone becomes depleted of ligands, which then have to be transported from the bulk of the vesicle. The crossover time, from which we can also obtain the reaction rate, is estimated from the full solution to be

$$t_{sw} = \frac{D}{(k_{on}a)^2}, \tag{1}$$

Consequently, if $\rho_l^0/\rho_r<1$ for $t < t_{sw}/4$, the time evolution of the area is quadratic (see Fig. S2 and Supporting Material for the derivation) and given by

$$A(t) = \pi\left(\frac{\rho_l^0}{\rho_r}\right)^2 k_{on}^2 a^2 t^2. \tag{2}$$

Interestingly, Eq. 2 also emerges from the solution for the reaction-limited kinetics and can be applied for $\rho_l^0/\rho_r>1$.

Due to the finite size of the vesicle, however, the growth will saturate as the system approaches a thermodynamic equilibrium (18). Actually, from t_{sat} (Eq. S26), the concentration of free ligands in the entire vesicle will begin to drop. This will affect the dynamics of growth in a way that is not accounted for in modeling (29–31), where one typically assumes the constant binder density (Eq. S2) at the rim. Actually, the smaller the number of ligands in the vesicle compared with the number of receptors (and formed bonds), the shorter is the reaction-limited regime and the quicker is the expansion of the depletion zone over the area of the entire vesicle. Hence, the finiteness will more strongly affect the diffusion-limited regime, which therefore should not be used to directly extract the diffusion constant of the ligand.

The crossover from the quadratic to the linear regime is clearly seen in our fastest neutravidin-biotin system (Fig. 1), as well as for the slower integrin-RGD binding (Fig. S4). The binding rate is obtained from both Eq. 1 and Eq. 2, as shown in Table 1. In principle, the two approaches provide relatively similar k_{on}-values. However, the results obtained with Eq. 2 may underestimate the rate by up to 50%. This is because the fits are extended to t_{sw}, which for fast processes may still be beneficial due to the limited time resolution of sampling. On the other hand, k_{on} obtained from the Eq. 1 agrees excellently with the values obtained from the fits of the full solution of the diffusion problem (Eq. S16). This is despite relatively large uncertainties in determining t_{sw}, and is due to the square-root dependency of the rate on this typical time.

Regardless of the abovementioned uncertainties, it is interesting that the difference in the binding rates between floppy and tense vesicles (neutravidin-biotin system) is significant. As was previously predicted theoretically (32,33),

TABLE 1 Association rate k_{on} in units of s^{-1} from experiments

	ρ_l^0/ρ_b	Eq. 1	Eq. 2
Biotin (floppy)	0.4	$(1.8 \pm 0.2)\cdot 10^3$	$(1.5 \pm 0.03)\cdot 10^3$
Biotin (tense)	0.4	$(1.2 \pm 0.1)\cdot 10^3$	$(0.6 \pm 0.02)\cdot 10^3$
RGD (1% PEG)	5.9		$(7.9 \pm 0.2)\cdot 10^1$
RGD (3% PEG)	5.9		$(6.0 \pm 0.1)\cdot 10^0$
sLe^x	59		$(4.1 \pm 0.1)\cdot 10^{-1}$

See Supporting Material for details and calculation of the error bars.

larger fluctuations of vesicle membrane increase the association rate k_{on} because encounters between ligands and receptors are more frequent.

Even more prominent is the change in the binding rate due to the presence of repelling polymers (PEG) mimicking the cellular glycocalyx. We incorporated these polymers at concentrations of 1 mol% and 3 mol% into vesicles carrying RGDs binding to integrins and found that k_{on} was one order of magnitude lower for vesicles with more PEG (Table 1). This clearly demonstrates that repelling molecules affect not only the thermodynamic equilibrium but also the rates for bond formation. In addition, the reported rate (1% PEG) is in full agreement with the rates extracted from the set of growth curves (19) where the concentration of RGD in the vesicles was varied systematically to induce the change from the diffusion-limited regime to the reaction-limited one (see Fig. S5 and Table S1 in the Supporting Material).

The condition for reaction-limited growth (second column in Table 1) is also very well satisfied for the slowest sialyl Lewis^x binding to E-selectin (20). As expected, the growth curves are well fitted with the parabola (for an example, see Supporting Material) corresponding to Eq. 2. This rate is of the same order of magnitude as the previously reported binding rates of membrane-bound P and L selectins (11) measured by the micropipette technique (10).

Here, we have presented a new (to our knowledge) strategy to measure the association constant k_{on} from adhesion growth curves. We used well-controlled cell models with three different kinds of ligand-receptor pairs to demonstrate proof of principle. We obtained the highest k_{on}-values for the energetically strongest bonds. The results suggest a mechanism that could be relevant for the control of cell adhesion dynamics, namely, the membrane shape fluctuations, which increase the association rate (32,33) when enhanced. On a similar note, we find that repelling polymer cushions, which were previously used to modulate unspecific GUV adhesion (20,34) as well as to influence bond formation in the context of surface-surface interactions (14,20), directly influence the association rate. This result is also interesting in the context of cells, as it suggests that bonds between binding pairs with long extracellular domains (e.g., as selectin-PSLG links) could form rapidly. In contrast, the links with integrins (hidden in the glycocalyx) should be very slow. These hypotheses are further supported by the fact that cells regulate both the membrane fluctuations and the thickness of the glycocalyx (22).

Interestingly, although they differ by at least an order of magnitude, the association rates for the integrin-RGD binding and the recognition of sialyl Lewis^x motifs by E-selectin are relatively low. This suggests that at physiological concentrations, the reaction-limited regimes could extend for a very long time before entering the diffusive regime. For example, for the sialyl Lewis^x binding to E-selectin, this time is on the order of 10^5 s, which is beyond the timescale of a cell or a vesicle. This suggests that a diffusion-limited behavior could not be relevant for cell adhesion with these two binding pairs unless extreme crowding effects would affect the recruitment of proteins to adhesion patches, which does not seem to be the case.

SUPPORTING MATERIAL

Supplemental Material, five figures, and one table are available at http://www.biophysj.org/biophysj/supplemental/S0006-3495(14)01116-3.

ACKNOWLEDGMENTS

We thank B. Lorz and Z. Guttenberg for providing some of the experimental data, and D. Schmidt for useful discussions.

A.S.S. and T.B. received funding from the European Research Council (Starting Grant 2013-337283) and Research Training Group 1962 at Friedrich-Alexander-Universität Erlangen.

REFERENCES and FOOTNOTES

1. Nguyen-Duong, M., K. W. Koch, and R. Merkel. 2003. Surface anchoring reduces the lifetime of single specific bonds. *Europhys. Lett.* 61:845–851.
2. Wu, Y., J. Vendome, …, B. Honig. 2011. Transforming binding affinities from three dimensions to two with application to cadherin clustering. *Nature.* 475:510–513.
3. Schmidt, D., T. Bihr, …, A.-S. Smith. 2012. Coexistence of dilute and densely packed domains of ligand-receptor bonds in membrane adhesion. *Europhys. Lett.* 99:38003.
4. Evans, E., and K. Ritchie. 1997. Dynamic strength of molecular adhesion bonds. *Biophys. J.* 72:1541–1555.
5. Seifert, U. 2000. Rupture of multiple parallel molecular bonds under dynamic loading. *Phys. Rev. Lett.* 84:2750–2753.
6. Erdmann, T., S. Pierrat, …, U. S. Schwarz. 2008. Dynamic force spectroscopy on multiple bonds: experiments and model. *Europhys. Lett.* 81:48001.
7. Krobath, H., B. Rozycki, …, T. R. Weikl. 2009. Binding cooperativity of membrane adhesion receptors. *Soft Matter.* 5:3354–3361.
8. Alón, R., D. A. Hammer, and T. A. Springer. 1995. Lifetime of the P-selectin-carbohydrate bond and its response to tensile force in hydrodynamic flow. *Nature.* 374:539–542.
9. Lorenz, B., L. Álvarez de Cienfuegos, …, A. Janshoff. 2012. Model system for cell adhesion mediated by weak carbohydrate-carbohydrate interactions. *J. Am. Chem. Soc.* 134:3326–3329.
10. Chesla, S. E., P. Selvaraj, and C. Zhu. 1998. Measuring two-dimensional receptor-ligand binding kinetics by micropipette. *Biophys. J.* 75:1553–1572.
11. Chen, W., E. A. Evans, …, C. Zhu. 2008. Monitoring receptor-ligand interactions between surfaces by thermal fluctuations. *Biophys. J.* 94:694–701.
12. Huang, J., V. I. Zarnitsyna, …, C. Zhu. 2010. The kinetics of two-dimensional TCR and pMHC interactions determine T-cell responsiveness. *Nature.* 464:932–936.
13. Huppa, J. B., M. Axmann, …, M. M. Davis. 2010. TCR-peptide-MHC interactions in situ show accelerated kinetics and increased affinity. *Nature.* 463:963–967.
14. Robert, P., A. Nicolas, …, L. Limozin. 2011. Minimal encounter time and separation determine ligand-receptor binding in cell adhesion. *Biophys. J.* 100:2642–2651.

15. Zarnitsyna, V., and C. Zhu. 2012. T cell triggering: insights from 2D kinetics analysis of molecular interactions. *Phys. Biol.* 9:045005.

16. Fenz, S. F., T. Bihr, …, A.-S. Smith. 2011. Switching from ultraweak to strong adhesion. *Adv. Mater.* 23:2622–2626.

17. Jeppesen, C., J. Y. Wong, …, C. M. Marques. 2001. Impact of polymer tether length on multiple ligand-receptor bond formation. *Science.* 293:465–468.

18. Smith, A., and U. Seifert. 2007. Vesicles as a model for controlled (de-) adhesion of cells: a thermodynamic approach. *Soft Matter.* 3:275–289.

19. Boulbitch, A., Z. Guttenberg, and E. Sackmann. 2001. Kinetics of membrane adhesion mediated by ligand-receptor interaction studied with a biomimetic system. *Biophys. J.* 81:2743–2751.

20. Lorz, B. G., A.-S. Smith, …, E. Sackmann. 2007. Adhesion of giant vesicles mediated by weak binding of sialyl-LewisX to E-selectin in the presence of repelling poly(ethylene glycol) molecules. *Langmuir.* 23:12293–12300.

21. Fenz, S. F., and K. Sengupta. 2012. Giant vesicles as cell models. *Integr. Biol. (Camb.).* 4:982–995.

22. Sackmann, E., and A.-S. Smith. 2014. Physics of cell adhesion: some lessons from cell-mimetic systems. *Soft Matter.* 10:1644–1659.

23. Fenz, S. F., A.-S. Smith, …, K. Sengupta. 2011. Inter-membrane adhesion mediated by mobile linkers: effect of receptor shortage. *Soft Matter.* 7:952–962.

24. Limozin, L., and K. Sengupta. 2009. Quantitative reflection interference contrast microscopy (RICM) in soft matter and cell adhesion. *ChemPhysChem.* 10:2752–2768.

25. Cuvelier, D., and P. Nassoy. 2004. Hidden dynamics of vesicle adhesion induced by specific stickers. *Phys. Rev. Lett.* 93:228101.

26. Cuvelier, D., M. Théry, …, L. Mahadevan. 2007. The universal dynamics of cell spreading. *Curr. Biol.* 17:694–699.

27. Brochard-Wyart, F., and P. G. de Gennes. 2002. Adhesion induced by mobile binders: dynamics. *Proc. Natl. Acad. Sci. USA.* 99:7854–7859.

28. Reister-Gottfried, E., K. Sengupta, …, A.-S. Smith. 2008. Dynamics of specific vesicle-substrate adhesion: from local events to global dynamics. *Phys. Rev. Lett.* 101:208103.

29. Shenoy, V. B., and L. B. Freund. 2005. Growth and shape stability of a biological membrane adhesion complex in the diffusion-mediated regime. *Proc. Natl. Acad. Sci. USA.* 102:3213–3218.

30. Freund, L., and Y. Lin. 2004. The role of binder mobility in spontaneous adhesive contact and implications for cell adhesion. *J. Mech. Phys. Solids.* 52:2455–2472.

31. Gao, H., W. Shi, and L.-B. Freund. 2005. Mechanics of receptor-mediated endocytosis. *Proc. Natl. Acad. Sci. USA.* 102:9469–9474.

32. Bihr, T., U. Seifert, and A.-S. Smith. 2012. Nucleation of ligand-receptor domains in membrane adhesion. *Phys. Rev. Lett.* 109:258101.

33. Hu, J., R. Lipowsky, and T. R. Weikl. 2013. Binding constants of membrane-anchored receptors and ligands depend strongly on the nanoscale roughness of membranes. *Proc. Natl. Acad. Sci. USA.* 110:15283–15288.

34. Sengupta, K., and L. Limozin. 2010. Adhesion of soft membranes controlled by tension and interfacial polymers. *Phys. Rev. Lett.* 104:088101.

Supplementary Information

Association rates of membrane-coupled cell adhesion molecules

Timo Bihr[1,2], Susanne Fenz[3,4], Erich Sackmann[5], Rudolf Merkel[3], Udo Seifert[2], Kheya Sengupta[6] and Ana-Sunčana Smith[1,7]

[1]Institut für Theoretische Physik and the Excellence Cluster: EAM, FAU, Erlangen, Germany; [2]II. Institut für Theoretische Physik, Universität Stuttgart, Germany; [3]Institute of Complex Systems 7: Biomechanics Forschungszentrum Jülich, Germany; [4]Department of Cell and Developmental Biology, Theodor-Boveri-Institute, Universität Würzburg, Germany; [5]Physics Department, Biophysics E22, Technische Universität München, Germany; [6] Aix-Marseille Université, CNRS, CINaM UMR 7325, Marseille, France; [7]Institute Ruđer Bošković, Division of Physical Chemistry, Zagreb, Croatia.

Theoretical Methods

Defining the Extended Stefan Problem

We consider a giant unilamellar vesicle that placed above a substrate, forms a contact zone where mobile ligands (initial density in the vesicle membrane ρ_l^0) can bind to immobile receptors (size a and density ρ_r on the substrate). Each bond deforms the membrane locally and pulls the membrane closer to the substrate (figure SI 1), which promotes the formation of a radially growing domain (bond density ρ_b). The deformation of the membrane at the rim brings free ligands in that region closer to the substrate, which then enhances the probability of binding at the edge of the domain. As the nucleation dynamics is in the current systems much slower than the spreading dynamics of a domain, only one (at most two) domains develop within the contact zone. In the model below, we assume that all receptors within a domain are bound, i. e. $\rho_b = \rho_r$.

The growth of such a domain can be regarded as a variant of the Stefan diffusion problem. We start by describing the flux of ligands, which are exploring the vesicle membrane with diffusion constant D, by the usual diffusion equation

$$\frac{\partial \rho_l(x,t)}{\partial t} = D\frac{\partial^2 \rho_l(x,t)}{\partial x^2}. \qquad \text{(SI 1)}$$

Here, $\rho_l(x,t)$ is the time dependent density profile of the ligands around the domain.

We, furthermore, set the number of binding events to be proportional to the density at the rim and to the association rate k_{on}, and equal to the diffusive flux at the rim. This implies

$$k_{\text{on}} a \rho_l\left(R(t),t\right) = D\left.\frac{\partial \rho_l(x,t)}{\partial x}\right|_{x=R(t)}, \qquad \text{(SI 2)}$$

where $R(t)$ is the radius of the domain. This expression should be valid as long as the edge of the expanding domain does not "move into" the concentration gradient. This is generally fulfilled because the motion of the rim and the relaxation of the concentration gradient is set by the diffusion of binders to the rim.

The above choice of the boundary condition is different to the usual approach where the density of ligands at the rim of the domain is fixed, as shown previously (refs. (29-31) of the main text). In the limit of infinite reaction rates, the solutions of our boundary conditions converge to the solution of the diffusion equation with the fixed boundary conditions. Furthermore, in the long time limit, the results obtained with the two approaches are asymptotically identical. However, using eq. (SI 2) allows us to explain the experimentally observed, short time quadratic regime of growth that precedes the diffusion limited growth.

The stated equation needs to be coupled to the growth of the domain, which is proportional to the flux of the ligands at the rim into the domain and the average distance between the bonds in the domain $1/\rho_r$ (see also refs. (29-31) of the main text). Therefore

$$\frac{\partial R(t)}{\partial t} = \frac{D}{\rho_r}\left.\frac{\partial \rho_l(x,t)}{\partial x}\right|_{x=R(t)} \text{ with } R(0) = R_0 \equiv 0. \qquad \text{(SI 3)}$$

Here, we set the initial radius of the domain to zero.

The above presented variation of the Stefan problem can be solved if the density of ligands is set at $t = 0$ and at infinite distance from the domain to

$$\rho_l(x, t=0) = \rho_l^0, \qquad \text{(SI 4)}$$

and

$$\lim_{x\to\infty} \rho_l(x,t) = \rho_l^0, \qquad \text{(SI 5)}$$

respectively.

Solving the Extended Stefan Problem

In order to solve the system of equation given by eqs. (SI 1)-(SI 5), we convert it to the co-moving frame and introduce the substitution

$$y = x - R(t). \qquad \text{(SI 6)}$$

In this frame, we obtain the diffusion equation

$$\frac{\partial \rho_l(y,t)}{\partial t} = D\frac{\partial^2 \rho_l(y,t)}{\partial y^2} + \frac{\partial R(t)}{\partial t}\frac{\partial \rho_l(y,t)}{\partial y}, \qquad \text{(SI 7)}$$

the adapted boundary condition

$$\rho_l\left(0\right) = \frac{D}{k_{\text{on}} a}\left.\frac{\partial \rho_l(y,t)}{\partial y}\right|_{y=0}, \qquad \text{(SI 8)}$$

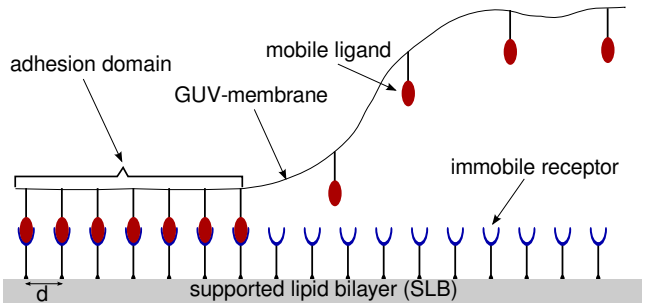

FIGURE SI 1 Sketch of the rim of the adhesion domain. The red ligands diffuse to the rim where they form bonds with the immobilize receptors increasing the size of the domain. The distance d between receptors is assumed to be uniform ($1/d = \rho_r$).

the moving boundary

$$\frac{\partial R(t)}{\partial t} = \frac{D}{\rho_r} \left. \frac{\partial \rho_l(y,t)}{\partial y} \right|_{y=0}, \tag{SI 9}$$

the initial condition

$$\rho_l(y, t=0) = \rho_l^0, \tag{SI 10}$$

and the boundary condition at infinity

$$\lim_{y\to\infty} \rho_l(y,t) = \rho_l^0. \tag{SI 11}$$

In the limit of close packing of receptors ρ_b, the second term in eq. (SI 7) disappears as the growth of the radius following eq. (SI 9) vanishes. In this case, the system reduces to an absorbing trap without moving boundaries and the boundary problem can be solved analytically (see for example Carslaw and Jaeger, Conduction of Heat in Solids), following a perturbation ansatz in ρ_l^0/ρ_r

$$\begin{aligned} \frac{\rho_l(y,t)}{\rho_l^0} &= \sum_{n=0}^{\infty} \varrho_l^n(y,t) \left(\frac{\rho_l^0}{\rho_r}\right)^n \\ \frac{\partial R(t)}{\partial t} &= \sum_{n=0}^{\infty} \frac{\partial R^n(t)}{\partial t} \left(1-\delta_{n,0}\right) \left(\frac{\rho_l^0}{\rho_r}\right)^n, \end{aligned} \tag{SI 12}$$

which provides us with a differential equation for every order of (ρ_l^0/ρ_r). The 0^{th} order term of the patch growth vanishes because, on this level of perturbation theory, the absorbing boundary is not moving. Here the differential equation for the concentration profile is

$$\frac{\partial \varrho_l^0(y,t)}{\partial t} = D \frac{\partial^2 \varrho_l^0(y,t)}{\partial y^2}, \tag{SI 13}$$

which is, as expected, the usual diffusion equation.

Even though the concentration of ligands is only correct to the 0^{th} order, the patch growth is obtained to the 1^{th} order

$$\frac{\partial R^1(t)}{\partial t} = D \left. \frac{\partial \varrho_l^0(y,t)}{\partial y} \right|_{y=0}. \tag{SI 14}$$

As suggested in Carslaw and Jaeger, Conduction of Heat in Solids (page 70ff) for this type of reduced boundary value problems, the solution for the ligand concentration profile reads

$$\begin{aligned} \frac{\varrho_l^0(y,t)}{\rho_l^0} &= \operatorname{erf}\left(\frac{y}{2\sqrt{Dt}}\right) + \\ &+ \exp\left(\frac{k_{\text{on}}^2 a^2 t + k_{\text{on}} a y}{D}\right) \operatorname{erfc}\left(\frac{y + 2k_{\text{on}} a t}{2\sqrt{Dt}}\right). \end{aligned} \tag{SI 15}$$

With this result, and with the help of eq. (SI 9), the time development of the radius of the adhesion domain can be calculated

$$R(t) \simeq \frac{\rho_l^0}{\rho_r} \left(\frac{D \exp\left(\frac{k_{\text{on}}^2 a^2 t}{D}\right) \operatorname{erfc}\left(\frac{k_{\text{on}} a t}{\sqrt{Dt}}\right)}{k_{\text{on}} a} + \frac{2\sqrt{Dt}}{\sqrt{\pi}} \right). \tag{SI 16}$$

This result is correct to the first order of ρ_l^0/ρ_r. The analysis of this solution indicates that the first term on the right hand side dominates the short time scales while the second term, proportional to $\sqrt{Dt}$ becomes relevant at the long time scales. The crossover between time t_{sw} (eq. (1) in the main text) between the two regimes is determined by comparing the terms depending on the reaction rate k_{on} (last term in eq. (SI 15) and the first term in brackets of eq. (SI 16))

$$t_{\text{sw}} = \frac{D}{(k_{\text{on}} a)^2}. \tag{SI 17}$$

The appearance of the two regimes is even more obvious after performing a Taylor expansion of eq. (SI 16) in $\sqrt{t}$ to the fourth order (i. e. to the second order in t), around $t = 0$

$$\begin{aligned} \frac{R(t)}{\rho_l^0} = \frac{R_0}{\rho_l^0} + \frac{k_{\text{on}} a t}{\rho_r} - \frac{4\left(\frac{k_{\text{on}}^2 a^2}{\rho_r}\right) t^{3/2}}{3\left(\sqrt{\pi D}\right)} \\ + \frac{\left(\frac{k_{\text{on}}^3 a^3}{\rho_r}\right) t^2}{2D} + O\left(t^{5/2}\right), \end{aligned} \tag{SI 18}$$

The obtained result contains no first order term ($\sqrt{t}$) which cancels out. Furthermore, it is easy to show the proportionality between the width of the concentration profile (eq. (SI 15)) and $\sqrt{Dt}$, as found in the arguments of the error function and the complementary error function. In other words, there is no stationary solution with a constant concentration profile. Instead, the solution of the extended Stefan problem has a constantly growing depletion zone. However, in the early stages of the domain growth, the depletion zone is not free of ligands, and its depth develops on a time scale of $D/(k_{\text{on}} a)^2$ (top panel in Fig. SI 2). Actually, only in the limit of an infinite effective binding rate, the ligand concentration around the adhesion domain would be zero from $t = 0$.

To summarize, we define two regimes for the growth behavior of the adhesion domain with the crossover at t_{sw} (lower

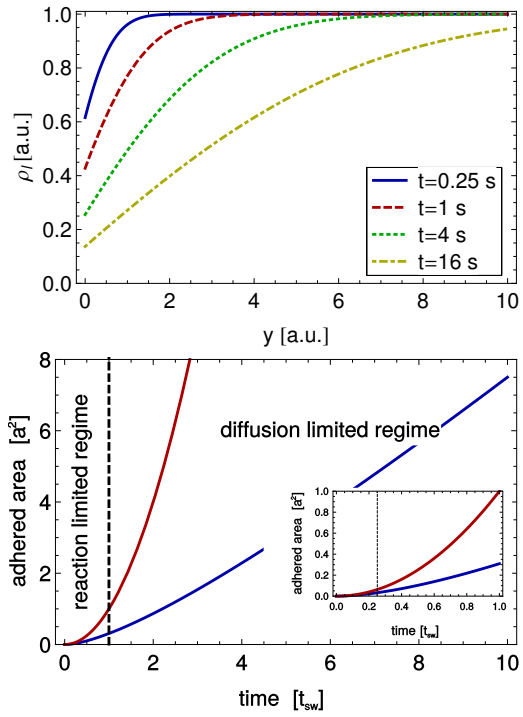

FIGURE SI 2 Top: Concentration profile as a function of the distance from the edge of the domain (set at $y = 0$) (SI 15). All parameters (D, k and a) were set to unity. Due to the finite reaction rate and uniform density of ligands prior to the formation of the domain, it takes some time before the concentration of ligands drops to zero at the edge of the adhesion domain. From this point, the concentration profile grows with $2\sqrt{Dt}$. Bottom: Theoretical growth curve for the adhered area (blue curve) and the initial quadratic curve (red curve). The length of the reaction limited regime depends on the initial ligand and receptor concentration as well as on the effective binding rate.

panel in Fig. SI 2). In the short time regime, the diffusion of ligands does not affect the growth because the surrounding of the adhesion domain is not yet depleted of binders and the growth is limited by the reaction kinetics. This is confirmed by eq. (SI 18), where the lowest order $\sqrt{t}$ disappears and the growth of the radius is linear (area is quadratic) for short times, i. e. reaction limited. From the first order term of eq. (SI 17), we derive the time development of the adhered area (eq. (2) from the main text),

$$A(t) = \pi \left(\frac{\rho_l^0}{\rho_r}\right)^2 {k_{\text{on}}}^2 a^2 t^2. \qquad \text{(SI 19)}$$

The asymptotic long time regime is only determined by the diffusion of ligands to the adhesion domain (i. e. it is diffusion limited). This also means that the first term of eq. (SI 16), which depends on the effective reaction rate k_{on}, can be neglected compared to the last, rate-independent term. This leads to a growth of the radius that is proportional to $\sqrt{Dt}$ (the domain area proportional in time) in the long time limit.

It should be noted that eq. (SI 19) also emerges from the consideration of the reaction limited dynamics, and consequently can be used also when $\rho_l^0/\rho_r > 1$, which is beyond the above presented perturbative scheme.

The reaction limited regime and the saturation time

We assume that the concentration of ligands is constant outside the adhered area and the number of reactions is proportional to the concentration at the rim of the adhered area and the reaction rate. Under those assumptions, the growth process can be described by

$$\frac{\partial N_b(t)}{\partial t} = k_{\text{on}} C_{\text{patch}}(t) a \left(\frac{N_{\text{t}} - N_b(t)}{A_{\text{V}}}\right), \qquad \text{(SI 20)}$$

where $N_b(t)$ is the number of bonds within the adhered area, N_t is the number of ligands at the beginning of the growth phase on the vesicle surface (i. e. $N_t = 4\pi r_V^2 \rho_l^0$), $C_{\text{patch}}(t)$ the circumference of the domain and A_{V} the surface of the vesicle. We transform equation (SI 20) by the relation

$$N_b(t) = \rho_b \frac{C_{\text{patch}}(t)^2}{2\pi} \qquad \text{(SI 21)}$$

to

$$\frac{\partial N_b(t)}{\partial t} = 2k_{\text{on}} \sqrt{\frac{\pi N_b(t)}{\rho_b}} a \left(\frac{N_{\text{t}} - N_b(t)}{A_{\text{V}}}\right), \qquad \text{(SI 22)}$$

which, now, only depends on the number of domain particles $N_b(t)$. This differential equation can be solved easily

$$N_b(t) = N_t \tanh^2\left(\frac{k_{\text{on}} a \sqrt{\pi N_t} t}{A_{\text{V}} \sqrt{\rho_b}}\right). \qquad \text{(SI 23)}$$

The solution has a quadratic onset of the growth curve which then saturates due to the finite size vesicle, even if the diffusion constant was infinite. Actually, the Taylor expansion to the second order in t yields an expression identical to the one shown in eq. (2) of the main text (i.e. eq. (SI 19)) (if the surface area A_{V} and the number of ligands N_t is replaced by $\rho_l^0 = A_{\text{V}}/N_t$).

From the full solution given by eq. (SI 23), we can read the typical saturation time

$$t_{\text{sat}} = \frac{A_{\text{V}} \sqrt{\rho_b}}{k_{\text{on}} a \sqrt{\pi N_t}} = \frac{2 r_V}{k_{\text{on}} a} \sqrt{\frac{\rho_b}{\rho_l^0}}. \qquad \text{(SI 24)}$$

This time tells when the concentration of free binders drops considerably on the vesicle surface if the diffusion is very fast and, thus, gives the lower bound of the time at which the growth will be affected by the finiteness of the system.

Experimental Methods

Sample preparation

GUVs (Giant unilamellar vesicle), carrying appropriate ligands, were prepared by electroswelling. Their interaction with

a specially prepared substrate exhibiting the corresponding receptor was monitored by micro-interferometric (RICM) imaging. The preparation process for each ligand-receptor pair is presented below:

For **the biotin-neutravidin pair**, GUVs consisting of SOPC (1-stearoyl-2-oleoyl-sn-glycero-3-phospho-choline) supplemented with 2 mol% DOPE-PEG 2000 (1,2-dioleoyl-sn-glycero-3-phospho-ethanolamine-N-(methoxy(polyethyl-eneglycol)-2000)) and varying amounts of DOPE-cap-biotin (1,2-dio leoyl-sn-glycero-3-phosphoethanolamine-N-(cap biotinyl)) were prepared in 230 mOsm/L sucrose solution via electroswelling. For micro-interferometry imaging, they were transferred to the observation chamber filled with 300 mOsm/L PBS. The bottom glass slide of the observation chamber had been coated with a supported lipid bilayer (bottom layer: pure SOPC, top layer: SOPC / 2 mol% DOPE-PEG 2000 / 5 mol% DOPE-cap-biotin) following the Langmuir Blodgett -Langmuir Schäfer technique and functionalized with neutravidin. It should be noted that although the neutravidin receptors were coupled to a fluid lipid bilayer, the receptors were effectively immobile due to crowding effects (Fenz et al., Langmuir, **25**:1074-1085 (2009)). The biotins covered an area of around 0.5 nm^2. Further details can be found in ref. (23) of the main text.

For **sialyl-Lewis^x binding to E-selectin**, the vesicles were prepared from an equimolar mixture of DMPC (1,2-dimyristoyl-sn-glycero-3-phosphocholine), cholesterol and 15 mol% of sialyl-Lewis^x-glyco-sphingolipids (C. Gege, S. Oscarson, and R.R. Schmidt, Tetrahedron Lett. **42**:377-380 (2001)). The vesicles were prepared by electro-swelling in a 170mOsm/L sucrose solution and placed in a 210 mOsm/L salt buffer (100 mM NaCl, 1 mM CaCl2, 1 mM NaN_3, 10 mM HEPES at pH of 7.2). The substrate was a clean glass cover slide (Merck, Germany) which was hydrophobized by immersion in a 1% toluene solution of aminosilanes (3-amino-propyltriethoxysilane) (both Fluka, Swiss) for 4 minutes at 60°C which was followed by rinsing with pure toluene and drying under N_2. Finally a recombinant form of the extracellular domain of human E-selectin (Calbiochem, San Diego, CA, USA) was physsorbed on the substrate by incubating the protein solution (maximum 5 µg/ml in the salt buffer) for two hours at room temperature, while the whole chamber was gently mixed on a shaking platform. After rinsing with buffer, the substrate was incubated at room temperature for one more hour with a buffer solution containing 3% of Blotting Grade Blocker Non-Fat Dry Milk (BioRad, Hercules, CA, USA) in order to prevent any direct contact of glass with the vesicle. Final careful rinsing of the slide with buffer completed the preparation. Here, the slex had a lateral size of around 10 nm^2. Further details on the preparation can be found in our earlier work (ref. (20) of the main text).

For **the RGD-integrin case**, giant vesicles were prepared from a 1:1 mixture of DMPC and cholesterol, to which 1 and 3 mol% of PDOPE-PEG 2000 were added. We also added 0.08–2 mol% of lipid-coupled cyclic hexapeptide containing an RGD sequence. Integrin $\alpha_{IIb}\beta_3$ receptors were prepared from blood platelets (Hu et al. Biochemistry **39**:12284–12294 (2000)) solubilized by Triton X100, and fixed on a clean glass substrate by physisorption during incubation. For this purpose, integrins were dissolved in Tris-buffer (20 mM Tris pH 7.25, 150 mM NaCl, 1 mM $MgCl_2$, 1 mM $CaCl_2$, 1 mM NaN_3, 0.01% Triton X100) to a concentration of 68 nM and the substrates were incubated in this solution for 1 h. In a second step, the substrates were incubated in a solution of 3 weight% bovine serum albumin in HEPES buffer (10 mM HEPES pH 7.25, 100 mM NaCl, 1 mM $CaCl_2$, 1 mM NaN_3). After each incubation, the substrates were thoroughly washed with HEPES buffer. The RGDs covered a size equivalent to the area covered by a lipid, hence, 0.5 nm^2 Further details of the preparation can be found in (ref. (19) of the main text).

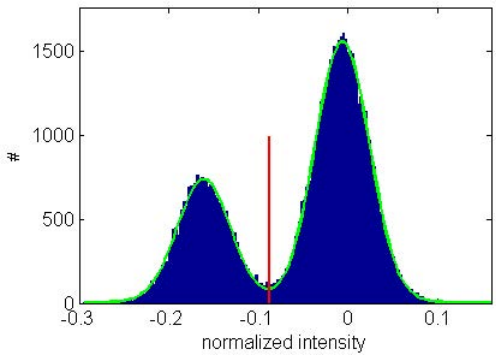

FIGURE SI 3 Histogram of intensities in a typical RICM image. The red line indicates the chosen threshold

Measuring setup and data analysis

In all cases, the observation chamber was covered with a glass slide to prevent changes in the buffer osmolarity due to evaporation. GUVs were located with the phase contrast mode of the microscope and observed during sedimentation. When the vesicles were close to the substrate the the contact zone was observed by reflection interference contrast microscopy (RICM) and the adhesion process was recorded at an image rate of 10 Hz (for more information on RICM see a recent review (ref. (24) of the main text). Thereby, the adhered area was determined by thresholding the intensity.

The threshold was extracted from the last image of the movie showing the adhered vesicle in its steady state. The histogram of all intensity values in the image exhibited two well separated peaks corresponding to the adhered and unadhered zones. Two Gaussians were fitted to the histogram. We defined the intersection between the two Gaussian distributions as the threshold value. Due to the well separated peaks (see Fig. SI 3), small variations from the threshold value did not result in substantial variations of the extracted area and did not affect the observed dynamics. After the completion

of the adhesion process, the vesicles were also recorded in phase contrast in order to measure their diameters.

Evaluation of the reduced volume of vesicles

Overall, our vesicles have a reduced value between 0.90 and 0.98 which was typically determined on the level of each swelling preparation, by measuring the radius of the vesicle in its equatorial plane in phase contrast. Combining this information with the measure of the radius of the contact zone, we were able to reconstruct the spherical cap describing the shape of the vesicle, and from there, to determine the reduced volume of the vesicle V_{red} following the expression

$$V_{red} = \frac{V_t}{V_i} \tag{SI 25}$$

where V_t denotes the volume of the truncated sphere and V_i the volume of the ideal sphere with the same surface area A. V_t, A, and V_i were calculated from the known radii of the vesicle measured in phase contrast r_V and of the contact zone measured in RICM r_{CZ}.

$$\begin{aligned} A &= 4r_V^2\pi - \pi\left(r_V - \sqrt{r_V^2 - r_{CZ}^2}\right)^2 \\ V_t &= \frac{4}{3}r_V^3\pi - \left[\frac{1}{3}\pi\sqrt{r_V^2 - r_{CZ}^2}\left(3r_V - \sqrt{r_V^2 - r_{CZ}^2}\right)\right] \\ V_i &= \frac{4}{3}\left(\sqrt{\frac{A}{4\pi}}\right)^3\pi \end{aligned} \tag{SI 26}$$

In the case of biotin-avidin bonds, where we investigated the role of membrane height fluctuations (see main text), we determined the reduced volume for each vesicle independently. Specifically, for floppy vesicles the reduced volume was 0.95 and for tense vesicles 0.97.

Extraction of reaction rates

Only data for which $t < t_{\text{sat}}$ was used in the analysis. If $\rho_l^0/\rho_r > 1$, eq. (2) (e.g. eq. (SI 19)) was systematically applied to all data using the least square method as implemented in *Mathematica 9.0*. Thereby, we used all data points from the beginning to the saturation (see also plots in figure SI 4).

In the case of $\rho_l^0/\rho_r < 1$, the reaction rate is first extracted from the crossover time eq. (SI 17) which is determined from the growth curves as time at which the long term linear regime fails to account for the data (i.e. the linear function going through the data points in the linear regime is around 15% smaller than the experimental values). Due to this procedure, the error in determining t_{sw} may be relatively large (up to 20% determined from small variations of the range of the linear fit). However, due to the square root dependence of the reaction rate on the cross-over time, the impact of this error on the accuracy of the rate is limited. Furthermore, the

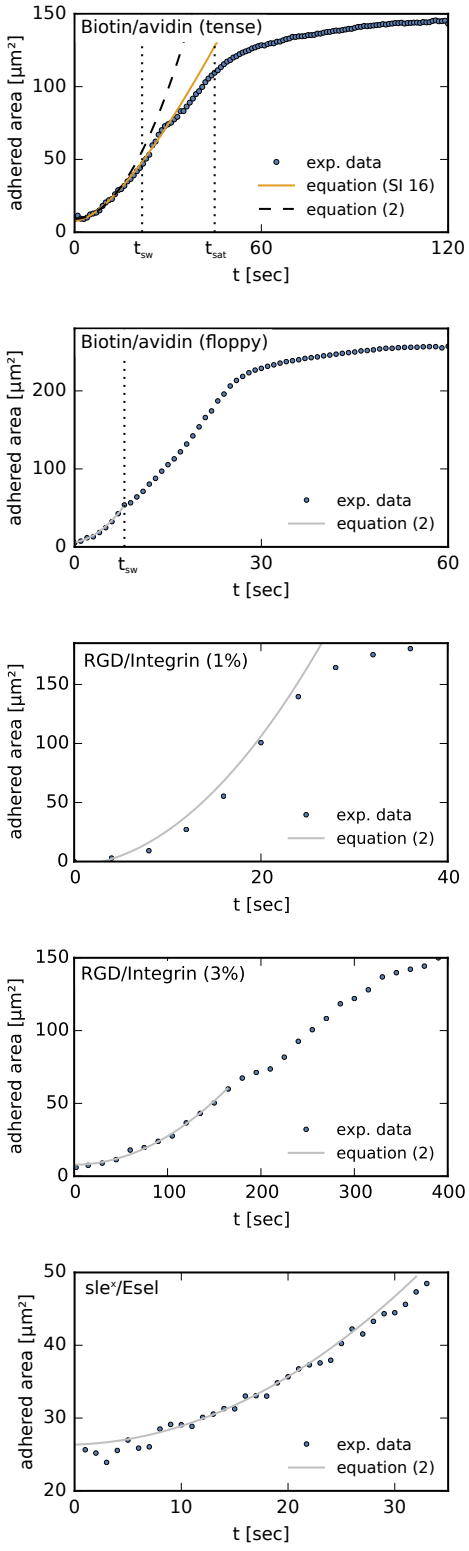

FIGURE SI 4 Characteristic growth curves of the adhered area for different binding pairs. In the top panel t_{sat} was estimated with eq. (SI 24) using $r_V = 10\mu m$ and $k_{\text{on}} = 10^3\ s^{-1}$

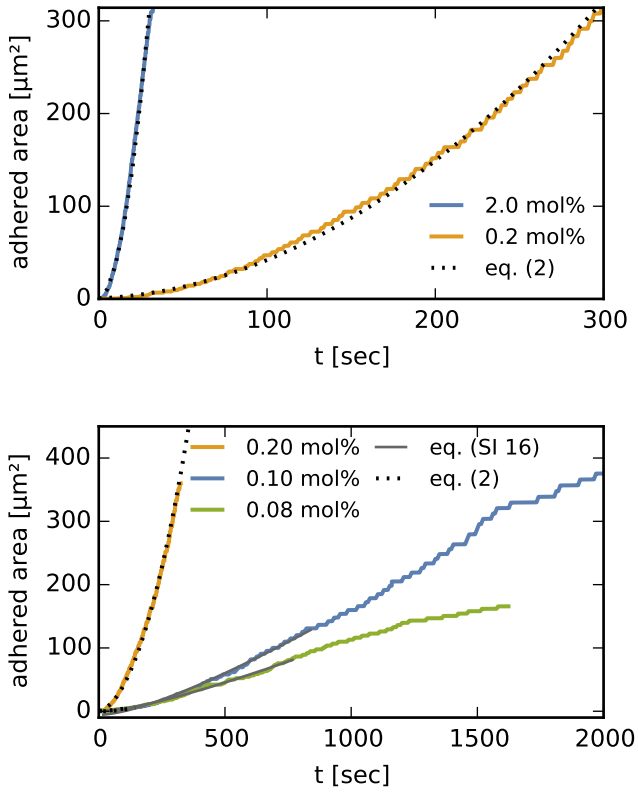

FIGURE SI 5 Top: Reaction limited curves and corresponding fits. This regime is relevant for large densities. Bottom: Diffusion limited curves and corresponding fits. Asymptotically, the curves are diffusion limited (i. e. linear in time) except for the largest density, where the rim of the contact zone is reached before the switch between reaction limited and diffusion limited behavior. Initially, the growth is reaction limited (i. e. the area grows quadratically in time). Here, the unit mol% is the percentage of lipids in the membrane carrying an RGD-molecule. Data taken from Boulbitch et al. (19) of the main text.

early stages of growth are fitted by the least square method to a parabola (eq. (2) of the main text). In principle, the convergence of eq. (2) to the true solution suggests that eq. (2) should be used only at very short time scales. However, due to the limited time resolution and a limited number of data points, the fitting interval was extended to t_{sw}. As a result the determined rates are systematically smaller than those obtained from t_{sw}, despite the good accuracy of the fit. We also applied the full solution of the Stefan problem to the data (eq. (SI 16)), which provides a rate that very well agrees with the rate obtained from t_{sw}. However, the complexity of the fitting function may render the fit unstable.

The reported errors were either determined from the fitting procedure (quadratic fits) or by linear error propagation (transition time).

Table SI 1 Values for the association rate obtained by different methods (in units of $[s^{-1}]$).

data set	eq. (1)	eq. (2)
0.08 mol%	61±6	64±1
0.10 mol%	66±7	46±1
0.20 mol%	-	78±2
2.00 mol%	-	79±1

Analysis of data published by Boulbitch et al. in Biophys. J. 81:2743

In order to show the applicability of the extended Stefan problem eq. (SI 1) to (SI 5), we apply our fitting procedure to data taken from Boulbitch et al. (19) of the main text. The growth curves can be seen in figure SI 5.

To show that the cross-over between two regimes is not a unique property of biotin-avidin binding discussed in the main text, we reanalyse growth curves published earlier. In this study, the authors systematically varied the density of ligands from the reaction to the diffusion limited regime for RGD-integrin binding (their preparation is identical to ours for 1% PEG content).

The extracted data clearly show the cross over behavior for the preparations with $\rho_l^0/\rho_r < 1$ and only a quadratic behavior for $\rho_l^0/\rho_r > 1$. Furthermore, we extract this reaction rates following the procedure outlined above and summarize the results in Table SI 1. Since only the density of ligands is changed between various preparations, the rate obtained from all curves should be the same (and equivalent to the rate reported in the main text).

Although direct fitting of eq. (SI 16) suggested a rate of $105 \pm 5s^{-1}$, the obtained results show a remarkable consistency. The systematic, however small variations in the results can be explained by saturation effects which may have affected the diffusion limited curves. This confirms our hypothesis, that the growth at low ligand densities can be described by our extended Stefan problem, whereas at high ligand densities the growth is reaction limited.